POLITECNICO DI TORINO
Repository ISTITUZIONALE

Design and Characterization of a Textile Electrode System for the Detection of High-Density sEMG

(Article begins on next page)

16 July 2022

Design and Characterization of a Textile Electrode System for the Detection of High-Density sEMG

Giacinto Luigi Cerone, *Member, IEEE*, Alberto Botter, *Member, IEEE*, Taian Vieira, and Marco Gazzoni, *Member, IEEE*

Abstract—**Muscle activity monitoring in dynamic conditions is a crucial need in different scenarios, ranging from sport to rehabilitation science and applied physiology. The acquisition of surface electromyographic (sEMG) signals by means of grids of electrodes (High-Density sEMG, HD-sEMG) allows obtaining relevant information on muscle function and recruitment strategies. During dynamic conditions, this possibility demands both a wearable and miniaturized acquisition system and a system of electrodes easy to wear, assuring a stable electrode-skin interface. While recent advancements have been made on the former issue, detection systems specifically designed for dynamic conditions are at best incipient. The aim of this work is to design, characterize, and test a wearable, HD-sEMG detection system based on textile technology. A 32-electrodes, 15 mm inter-electrode distance textile grid was designed and prototyped. The electrical properties of the material constituting the detection system and of the electrode-skin interface were characterized. The quality of sEMG signals was assessed in both static and dynamic contractions. The performance of the textile detection system was comparable to that of conventional systems in terms of stability of the traces, properties of the electrode-skin interface and quality of the collected sEMG signals during quasi-isometric and highly dynamic tasks.**

Index Terms—**Electrode-skin interface, EMG acquisition systems, high-density EMG, textile electrodes.**

I. Introduction

THE interest for wearable devices in the biomedical field is rapidly growing, stimulated by the development of key-enabling technologies like sensor, microelectronics, communication technology, and data processing techniques. The advantages of wearable systems with respect to traditional devices are a higher freedom of movements and unobtrusiveness provided to the wearer, the comfort and the possibility of long-term and continuous monitoring.

The monitoring of electrophysiological signals such as ECG, EEG, and EMG is of paramount importance for many biomedical applications: clinical diagnosis [1], health monitoring, and human-machine interaction [2]. Conventionally, biopotential signals are measured by "wet" electrodes. Wet electrodes adopt an electrolytic conductive gel to optimize the electrode-skin contact and impedance and an adhesive pad to obtain a stable contact with the skin. However, wet electrodes have some limitations in long-term monitoring because of skin irritation and degradation of the electrode-skin interface over time.

Different technologies for dry electrodes have been investigated in the last years [3], [4] to overcome the aforementioned limitations of traditional wet electrodes in long term and home monitoring of electrophysiological signals. They can be grouped in: microneedles-based electrodes [5], capacitive electrodes [6], tattoo electrodes [7]–[9], and textile electrodes [3], [10]–[12].

Textile electrodes received considerable attention because they can be easily integrated into garments to enable long-term monitoring. Textile electrodes are usually fabricated using standard fabric manufacturing techniques such as knitting, weaving, embroidery of conductive fibers, or they are manufactured by applying conductive materials onto finished textiles with various techniques like electroplating, physical vapor deposition, chemical polymerization, coating and printing methods [13], silver nanowires (AgNWs) and polydimethylsiloxane (PDMS)-based electrodes [14].

While research mainly focused on the development of textile electrode for ECG [11], the possibility to continuously assess muscle activity through electromyography (sEMG) is of high interest. EMG is used in a wide range of applications from physical rehabilitation to sport science, from ergonomics to prosthetics and robotic exoskeletons.

Several works investigated different techniques for textile sEMG electrode development [10], [14], [15]. Textile EMG electrodes embedded in garments have been used in the monitoring of muscle activity during daily and sport activities [16]–[22], rehabilitation settings [16], [23], [24], in prosthetic control [25]–[28]. In most of these technological solutions, individual, EMG textile electrodes cover a large area of the muscle (e.g. 42 cm^2 [18]; 12 cm^2 [29]), which allows

optimizing the electrode-skin contact and the quality of the detected signals.

In the last two decades, high-density EMG (HD-sEMG) gained considerable attention in different fields. HD-sEMG adopts several closely spaced electrodes over the skin over-lying the muscle to provide a two-dimensional representation of the electric potentials generated by the muscle under investigation. HD-sEMG provides more information than classic bipolar recordings about peripheral and central properties of the neuromuscular system [30]–[35]. Despite these advantages, HD-sEMG setup is cumbersome and time-consuming, limiting its application to laboratory studies and quasi-static contractions.

Recently, some significant steps forward in the miniaturization of HD-sEMG acquisition system have been reported in literature [36], opening the possibility to acquire high-quality signals during free movements whereas a HD-sEMG detection system easy to apply and assuring a stable electrode-skin interface is still not available. Typically, HD-sEMG detection systems consist of a flexible printed circuit board (PCB) with silver pads acting as electrodes. The flexible PCB is applied to the skin using a perforated, bi-adhesive foam manually filled with a conductive paste [12]. This solution is time consuming and requires a careful preparation to avoid electrode-skin contact problems. A solution to these issues could be represented by a textile grid of electrodes integrated into a garment to simplify donning and doffing. Conversely, fabric-based detection systems may suffer from coarse electrode skin contacts, resulting in the detection of noise and power line interference. Only a few preliminary works in literature investigated the development of HD-sEMG textile systems [25], [37]. In both cases the electrode-grid was not characterized in terms of electrical characteristics and electrode-skin interface and it was mainly used to assess sEMG activity distribution under the electrodes. Farina *et al.* evaluated the feasibility of using a sleeve with embedded high-density electrode grids for the control of active hand prostheses [25]. The goal was verified based on the classification accuracy of nine hand/wrist movements using wavelet coefficients extracted from sEMG signals. Although the authors observed a good classification accuracy ($89.1 \pm 1.9\%$), however, since signal acquisition was limited to isometric contractions and feature extraction and dimensionality reduction is performed before classification, it is not possible to infer details about the quality of electrode-skin interface and robustness of raw signals. Gazzoni *et al.* used a grid of 112 silver electrodes integrated into a stretchable textile sleeve to quantify the spatial distribution of sEMG activity of distinct forearm muscles during dynamic free movements of wrist and single fingers and the effect of hand position on such a distribution [37]. This solution was based on a mixed technique using circular silver electrodes connected to the amplifier through conductive wires embroidered into an elastic sleeve. The process to fabricate one single grid was fully manual, error prone, and time consuming without the possibility to be easily automated.

The aim of this work was to develop and characterize a wearable, dry-contact HD-sEMG detection system based on textile materials. In the design phase the following specifications were considered: a) easy of wearing and use, b) manufacturability for future small-scale production.

The system characterization was performed in terms of a) electric characteristics of the conductive traces, b) electrode-skin impedance assessment in different conditions, c) signal quality and robustness to movement artefacts during static and dynamic tasks.

II. Materials and Methods

A wearable HD-sEMG detection system composed of 32 electrodes (8 rows × 4 columns, 10 mm diameter) with 15 mm Inter-Electrode Distance (IED) was designed and prototyped. The electrode size and IED were chosen to sample sEMG signals from medium-large muscles, such as those of legs and arms [38].

A. Textile Grid Design

The textile grid is composed of three elements (Figure 1): 1) a polyamide/elastane fabric substrate, 2) a layer of silver electrodes and conductive traces deposited through a lamination process on a stretchable thermoplastic polyurethane (TPU) support (Intexar^{TM}, total thickness 75 μm), and 3) a flexible PCB adapter used to interface the grid with the EMG amplifier's inputs. A thin and light, 3D-printed grid of circular plastic pads is applied to the external layer to improve the mechanical stability of the electrode-skin contact. The polyamide/elastam substrate was used to: a) simplify the donning on and donning off of the electrode grid, b) apply an optimal pressure to the electrode on the skin to minimize movement artefacts and improve electrode-skin impedance, c) simplify the connection between the electrode grid and conditioning electronics.

The detection system layout was designed using the Altium Designer 19 EDA software. This layer comprises a grid of eight by four electrodes (10 mm diameter, surface area of 0.78 cm^2), inter-electrode distance: 15 mm center-to-center), a set of 32 pads (2.54 mm × 4.5 mm each) arranged in two rows along the long side of the electrode grid for the interconnection with the amplifier adapter, and the traces between the electrodes and the pads (width: 0.254 mm) (Figure 1.b).

The traces layout was not optimized against elastic stress (e.g. creating multiple coils structures) because the stress-tests (described in the paragraph 2.2) showed no significant alterations of the wire conductivity due to wire damage for deformations below 21%.

The layout of electrodes and wires was transferred to the Elastam textile support by lamination, using the Intexar^{TM} film (DuPont^{TM}, Delaware, USA). This material is generally used to create current driven heating dresses. The Intexar film is usually composed of five different stacked layers:
1. A Thermoplastic Polyurethane (TPU) laminate acting as bonding layer with the fabric;
2. A layer of silver acting as heat conductor;
3. A layer of carbon, placed only on the pads, used for current sensing applications;
4. An encapsulant, non-conductive layer used to fix layers together;
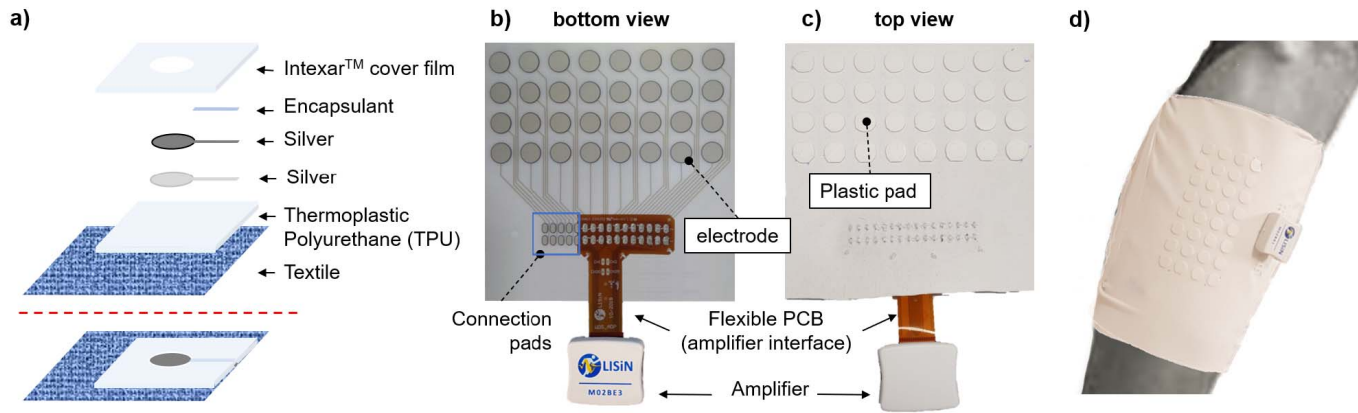5. A cover film acting as protecting layer.

Fig. 1. Textile grid structure composed of an Intexar^{TM} based film of Silver electrodes applied to an Elastam substrate. The stacked structure of the Intexar film (total thickness 75 μm) for one electrode and its connecting wire is shown in a). b) and c) show the bottom and top sides of the electrode grid, respectively. A flexible PCB is used to interface the grid with the HD-sEMG amplifier though a ZIF connector. The connection pads on the textile substrate (shown exposed in the blue box) are glued (silver-loaded glue 8331, MG Chemical Ltd, Canada) and sewed to the corresponding pads of the flexible PCB. A 3D-printed, flexible plastic grid of pads is applied on the back of the electrodes to improve electrode-skin contact. d) Textile grid of electrodes integrated into a sleeve applied to the shank of a subject and connected to a 32-channels wireless HD-sEMG amplifier [36].

In our prototype, the carbon layer on the pad and electrode areas was replaced with an additional silver layer (Figure 1.a), constituting the electrodes surface in contact with the skin, to improve the electrical properties of the electrode-skin interface [38]–[42].

The electrical connection between the textile grid and the acquisition system was obtained through an adapter consisting of a flexible ThinFlex^{TM} Printed Circuit Board (0.8 mm thick). The adapter was designed to be connected to a wireless and modular acquisition system for HD-sEMG detection during dynamic tasks (Meacs – LISiN, Politecnico di Torino, Italy [36], [43]). The adapter carries, on one end, 32 pads interfacing the textile and, on the other end, the connector for the HD-sEMG acquisition system (Molex 54104-3231, Molex Inc., Illinois, USA). Once aligned, the pads of the flexible PCB and the correspondent pads of the textile were individually sewed (Innovis 200 programmable sewing machine, Brother Machines, UK) with a polyester wire and then glued with a silver-loaded conductive glue (8331, MG Chemical Ltd, Canada). The polyester wire is not conductive, but it contributes to maintaining the contact between textile and PCB pads also in case of small cracks in the conductive glue. The interface between textile and PCB is shown in Figure 1.b and Figure 1.c.

As compared to gelled electrodes, textile electrodes with dry contact are characterized by a more unstable electrode-skin contact due to the absence of a sticking layer. Although appropriate electrode-skin contact may be achieved by tightening the dry electrodes with an elastic band, our experience suggests that the degree of tightening leading to the detection of signals with acceptable quality is often unbearable, especially during dynamic contractions. This issue is aggravated when we consider a grid of textile electrodes embedded into highly flexible layers, as local differences in pressure over the grid and changes in muscle shape may result in local differences in the quality of the electrode-skin contact [44]. To obtain a good electrode-skin contact using a comfortable tightening sleeve, a 3D-printed PLA plastic grid of pads (1 mm thick)

was laid on the back of the electrodes (Figure 1.c) and fixed with non-conductive silicon glue [44], [45]. Figure 1.d shows the textile grid of electrodes integrated into a sleeve applied to the shank of a subject and connected to a 32-channels wireless HD-sEMG amplifier [36].

B. Characterization of the Detection System

Three levels of characterization were identified and carried out:

1. *Electrical, In-System* – The electrical properties of the Intexar conductive layer and their stability to mechanical stress were evaluated;
2. *Electrode-Skin Interface* – The electrode-skin interface was characterized in terms of impedance and noise;
3. *EMG Detection* – The detection-amplifier system was used to acquire HD-sEMG signals in different experimental conditions involving both static and dynamic contractions.

1) Electrical, In-System, Characterization: One of the main concerns regarding textile-printed detection systems for biopotential acquisition is the stability of electrical conductibility of the traces connecting the electrodes and the amplifier [46], [47] when a stress is applied. The properties of the electrode-amplifier system (i.e. the electrode-skin impedance together with the input impedance of the front-end amplifier) shall not introduce distortion on the sEMG input signal [12], [41], [48], [49]. Usually, the impedance of the connecting cables is neglected in the electrode-amplifier model because it is characterized by low resistance (few Ohms) and negligible reactive components. In the case of textile-printed connections, the electrical model of the traces is not known a priori because stacking different films may introduce stray capacitances in the model and the electrical properties of the conductor films, in terms of resistance and inductance, depend on the length and cross-section of the connecting wires. Moreover, these parameters may vary with the deformation of the traces. Therefore, an electrical, in-system, characterization
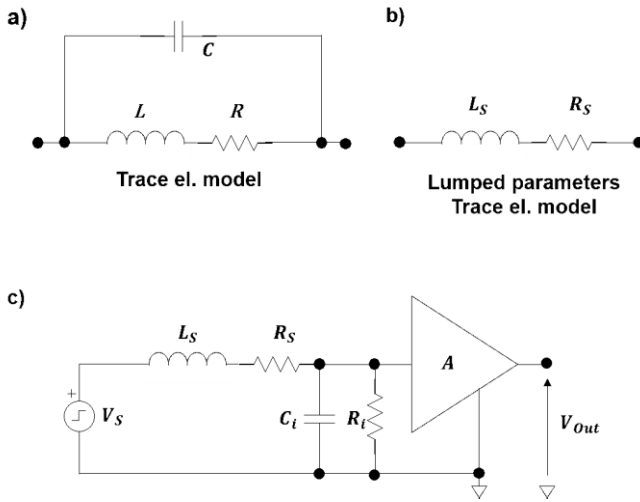
Fig. 2. a) Electrical model of a single, textile printed trace. The capacitor C represents a distributed stray capacitance between all textile's layers. b) Simplified, lumped parameters model of the textile trace. c) electrical model describing the coupling between a voltage source (V_S) used as test signal, a textile trace, and an oscilloscope used for the characterization of the trace's electrical properties. The input impedance of the amplifier is indicated by the C_i-R_i parallel circuit.

of the textile-printed traces was carried out to identify possible problems due to either the traces properties or the deformation of the textile detection system during use.

The electrical model of a single textile-printed trace is shown in Figure 2.a. It is composed of the resistor R and the inductor L, respectively modelling the electrical resistance and the auto-inductance coefficient of the conducting film, and a capacitor C, modelling the distributed stray capacitance between the films composing the Intexar^{TM} material.

Under the reasonable assumption that the bandwidth (B) of the signal of interest is much smaller than the natural frequency of the model f_0 (B $\ll$ f_0), it is possible to simplify the second-order model in Figure 2.a with a first-order lumped-element model composed by the R_S-L_S series circuit described in Figure 2.b, where:

$$R_s = \frac{R}{1 - LC\left(\frac{\omega}{\omega_0}\right)^2} \quad L_s = \frac{L}{1 - LC\left(\frac{\omega}{\omega_0}\right)^2} \quad for \ \omega \ll \omega_0$$

$$(1)$$

Figure 2.c shows the electrical model describing the coupling between one trace and the input stage of an oscilloscope used for measurements. The oscilloscope input impedance is represented as a R-C parallel circuit. Under these conditions, the trace-amplifier system is a second order RLC system, whose parameters damping factor ξ and natural pulsation ω_0 can be estimated as:

$$\xi = \frac{|ln(\hat{s})|}{\sqrt{\pi^2 + ln(\hat{s})^2}} \quad \omega_0 = \frac{\pi - acos(\xi)}{t_r\sqrt{1 - \xi^2}}$$

$$(2)$$

where V_S is the exciting step input signal, $\hat{s}$ is the overshoot and t_r is the 10%-90% rise time of the measured excitation response.
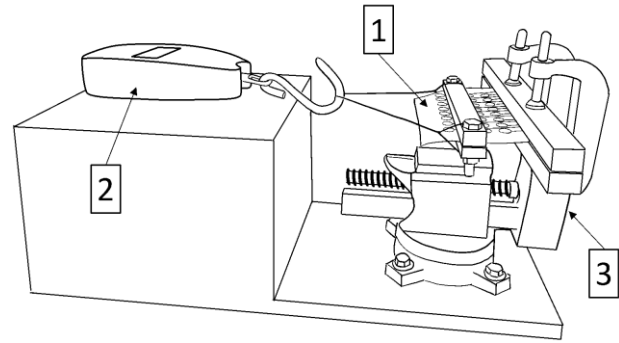

Fig. 3. Experimental setup used to characterize the changes in electrical properties of the textile traces due to longitudinal deformations. 1) The textile grid under test, 2) the digital dynamometer to measure the tensile force associated with the stress applied to the fabric, 3) the tensioning system.

The equivalent capacitance C and the auto-inductance L can be calculated as:

$$C = \frac{k}{1 - kL_S\left(\omega_0^2\right)} \quad L = L_S\left(1 - kL_S\left(\omega_0^2\right)\right) \quad (3)$$

where $k = \dfrac{R_S - R}{RL_S(\omega_0^2)}$

whereas the resistance R is measured by means of a multimeter (Fluke 175, Fluke Corp. - USA).

This electrical model was used to characterize the electrical properties of the textile-printed traces with and without longitudinal stress applied. The longitudinal stress condition was used to evaluate the electrical properties of the traces when stretching the grid (a condition likely occurring. during dynamic tasks or when donning the textile grid). To this end, a tensioning system was built (Figure 3). The system is composed of a mechanical clamp connected to two wood inserts in which the fabric is gripped. One end of the inserts was connected to a digital dynamometer (Lacor, Spain) to have a measurement of the tensile stress applied to the fabric and consequently to the traces. The deformation was progressively increased from 0% to 100% in steps of 3 %. For each step, the impedance of the wires was measured. Figure 3 shows the experimental setup.

2) Electrode-Skin Interface Characterization: The characterization of the electrode-skin interface was based on the measurement of the electrical impedance and noise. The electrode-skin contact can be modeled as an electrical impedance that, in the case of dry-contact silver electrode consists of a parallel R-C network with mostly non-polarizable effect (i.e. the resistive component prevails on the reactive one) in the sEMG bandwidth (10 Hz - 500 Hz) [4], [40], [42], [50]. The characterization of the electrical impedance at the electrode-skin interface is important because the coupling between the biopotential amplifier input stage and the electrode-skin system can lead to i) distortion and attenuation of the input signal due to the so-called "voltage divider effect" [34], [40], and ii) 50 Hz/60 Hz power line interference. The first problem can occur if the electrode-skin impedance in the sEMG frequency bandwidth is not negligible with respect to the amplifier input impedance in the same bandwidth. The latter problem is frequent if a 50 Hz/60 Hz common
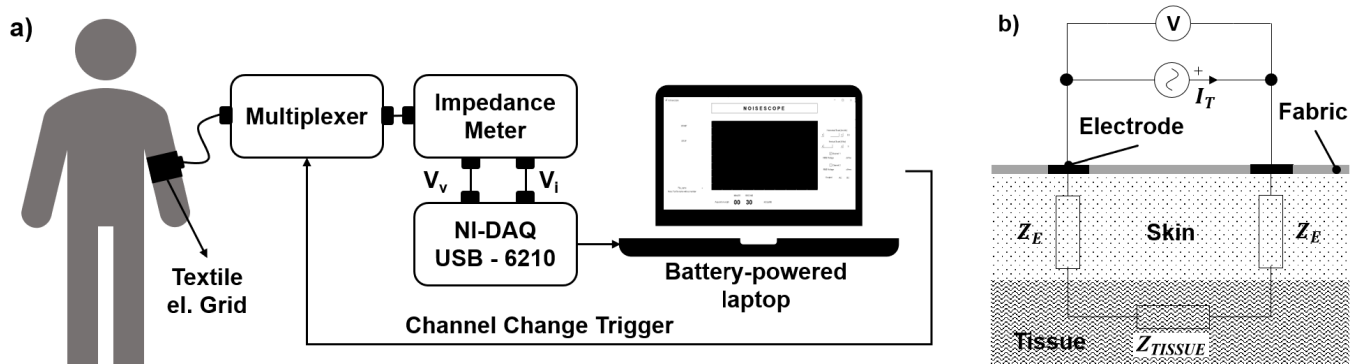
Fig. 4.   a) Experimental setup used to measure the electrode-skin impedance through a multi-channel and automatic impedance-meter designed at LISiN (Politecnico di Torino, Turin, Italy). The details about the characteristics of each block are described in the text. b) Detail of two electrode-skin interfaces and the related impedances (Z_E). Z_{TISSUE} is the impedance of the tissues underlying the skin.

mode signal due to the stray capacitive coupling between a subject and the power line is present, and the impedance unbalance between the exploring electrodes is not negligible with respect to the amplifier input impedance at the power line frequency [39]–[41], [49], [51].

Therefore, it is important to know the electrode-skin impedance value in the sEMG bandwidth and in particular at the power line frequency [12].

The electrode-skin impedance was measured between two identical electrodes. Considering the model showed in Figure 4.b and the fact that the properties of the skin below adjacent electrodes are presumably comparable, it is possible to assume a similar contribution of each electrode to the total, measured impedance. The impedance of the underlying tissues was not considered because its value (few hundreds of Ohm) is negligible with respect to the expected electrode-skin impedance (tens or hundreds of kilo-Ohm) in standard experimental conditions [52].

The impedance measurements were performed using a multi-channel and automatic impedance-meter designed at LISiN (Politecnico di Torino, Turin, Italy). The block diagram of the impedance-meter is shown in Figure 4.a. The instrument injects current through the impedance under-estimation and measures the resulting voltage (V_V). A sinusoidal input voltage signal V_I, provided by an internal oscillator with adjustable frequency and amplitude, is converted into a proportional current I_T ($V_I = k*I_T$) of 1 μA_{RMS} [53], [54]. V_I and the voltage drop across the impedance V_V are simultaneously acquired using a NI-DAQ USB-6210 acquisition board (National Instruments, Texas, USA) with 16-bit resolution and a sampling frequency of 10 kHz. Signals are displayed and stored on a battery-powered laptop. An integrated 32 channels programmable multiplexer connects two channels at a time to the impedance meter, allowing to automatically span the measurements over all the 32 channels of the textile grid. The channel switching operation is provided by a trigger signal generated by the laptop running the acquisition software. The entire system is floating with respect to ground to minimize the possible over-estimation of the impedance component at 50 Hz/60 Hz due to residual power line interface.

The impedance magnitude at a given frequency is calculated by the ratio $V_V/(V_I/k)$ (RMS values) for each frequency

(1 Hz resolution in the sEMG bandwidth). The resulting impedance Bode Plot was used to evaluate the electrode-skin impedance at 5 Hz and 50 Hz (Power Line frequency).

We characterized the electrode-skin impedance for different pressures applied on the electrodes and for two different skin preparations [52], [55]. The measures were performed on the Biceps Brachii of two subjects in two experimental conditions: without applying any skin treatment, and after a gentle scrub of the skin with a medical grade abrasive paste (Nuprep, Weaver and Company, Aurora, USA) [52]. This protocol was designed to investigate the expected range of variability of electrode-skin impedance in the best (skin treatment) and worst (no skin treatment) scenarios. In both cases, the skin was rinsed with water and dried before the application of the electrodes in order to remove superficial residuals (e.g. soap, sweat etc.). Two measures with different pressure applied to the electrodes were carried out for both skin-treatment conditions. In the first one the detection system was held in place with an elastic sport sleeve (Roadr, Decathlon, France). In the second one we applied a constant pressure of 30 mmHg by means of a blood pressure cuff covering the grid. This condition was used as a reference to compare the impedance values obtained using the elastic sleeve. In all conditions, measurements started five minutes after positioning the electrode grid on the skin.

The noise level at the electrode-skin interface was measured using a low noise (100 nV) biopotential amplifier developed at LISiN (Politecnico di Torino, Turin, Italy) and integrated into the impedance-meter device [56].

3) HD-sEMG Signals Detection: The experimental characterization of the textile electrode grid was aimed to demonstrate the quality of the detected sEMG signals in real-case scenarios. The study complied the principles outlined in the Helsinki Declaration of 1975, as revised in 2000. Informed consent was obtained from the subjects after providing detailed explanation of the study procedures.

Thirty-two monopolar sEMG signals were collected using a miniaturized wireless and modular 32 channel acquisition system for HD-sEMG (LISiN, Politecnico di Torino, Italy; [36]). Detected signals were transmitted to the receiver through an access point acting as a router. The acquisition system was connected to the textile grid through the adapter described in the Paragraph 2.1.

Impedance Map (kΩ)

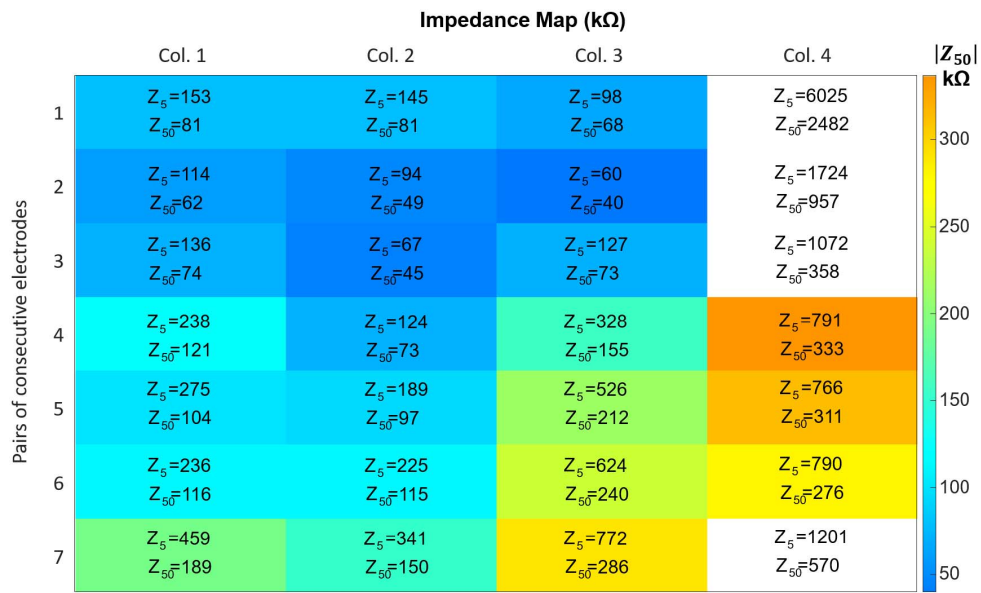|	Col. 1	Col. 2	Col. 3	Col. 4
1	Z_5=153 Z_{50}=81	Z_5=145 Z_{50}=81	Z_5=98 Z_{50}=68	Z_5=6025 Z_{50}=2482
2	Z_5=114 Z_{50}=62	Z_5=94 Z_{50}=49	Z_5=60 Z_{50}=40	Z_5=1724 Z_{50}=957
3	Z_5=136 Z_{50}=74	Z_5=67 Z_{50}=45	Z_5=127 Z_{50}=73	Z_5=1072 Z_{50}=358
4	Z_5=238 Z_{50}=121	Z_5=124 Z_{50}=73	Z_5=328 Z_{50}=155	Z_5=791 Z_{50}=333
5	Z_5=275 Z_{50}=104	Z_5=189 Z_{50}=97	Z_5=526 Z_{50}=212	Z_5=766 Z_{50}=311
6	Z_5=236 Z_{50}=116	Z_5=225 Z_{50}=115	Z_5=624 Z_{50}=240	Z_5=790 Z_{50}=276
7	Z_5=459 Z_{50}=189	Z_5=341 Z_{50}=150	Z_5=772 Z_{50}=286	Z_5=1201 Z_{50}=570

Fig. 5. Color map showing the impedance values at 5 Hz and 50 Hz (color scale) for all the pairs of adjacent electrodes along the four columns of the grid. White boxes indicate impedance value at 5 Hz above 1 MΩ.
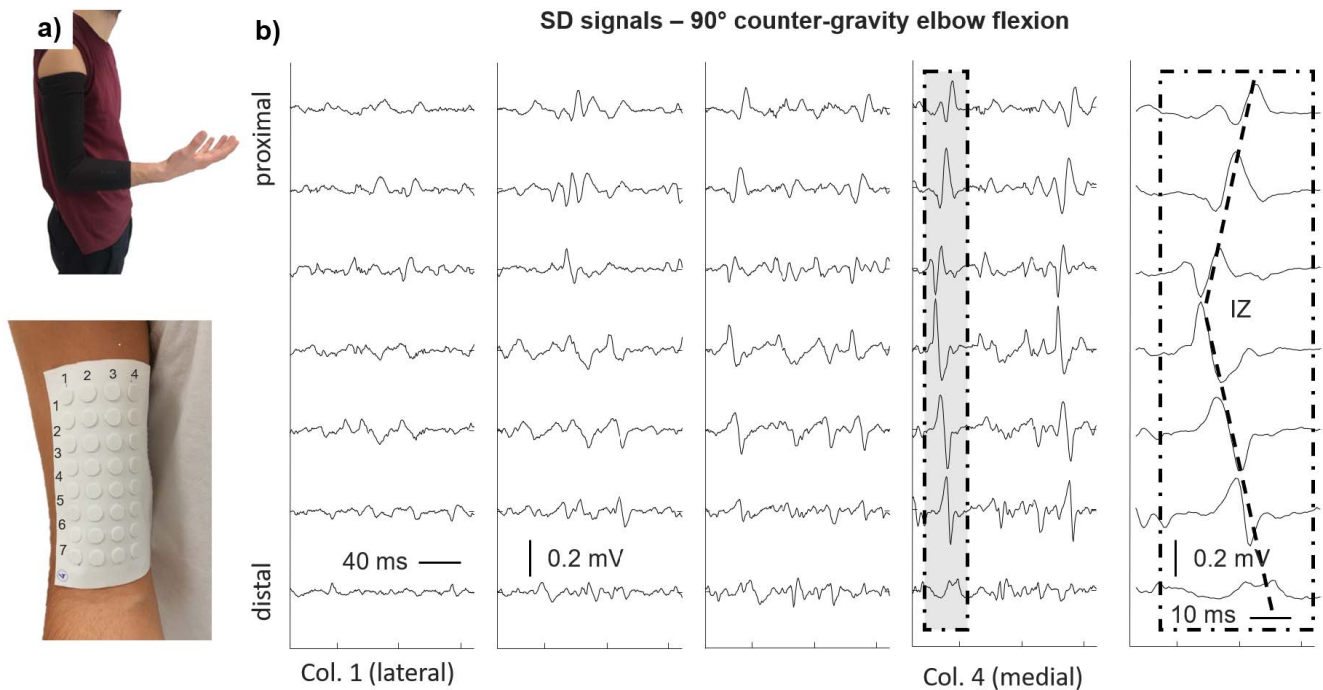

Fig. 6. Example of signals acquired during an isometric contraction. a) Shows the 32-electrodes textile grid applied to the biceps brachii muscle of a healthy subject and the electrode grid fixed to the subject arm using an elastic sleeve. b) Single differential sEMG signals collected from the Biceps Brachii muscle during a counter-gravity static contraction at 90° of elbow flexion. An expanded view of the signal epoch detected under Column 4 (shaded area) is shown in the right panel, where the propagation and the location of the innervation zone (IZ) can be appreciated.

Two experimental protocols including isometric and dynamic contractions were carried-out.

Counter Gravity Isometric Contraction: Monopolar HD-sEMG signals were collected from the biceps brachii muscle of a healthy subject (Male, Age 26, BMI: 22.2) using the textile grid of electrodes (8 rows × 4 columns, 15 mm inter-electrode distance). Skin was gently scrubbed with a medical grade abrasive paste (Nuprep, Weaver and Company, Aurora, USA). Columns of electrodes were aligned parallel to the muscle fibers and the grid was secured with an elastic sport sleeve (Roadr, Decathlon, France) (Figure 6.a). The subject was asked to sustain a counter-gravity contraction holding the elbow joint flexed at 90°. Given our interest focused on the qualitative assessment of experimental signals, we limited data collection to a functional condition. Even though we did not control for movement of the elbow joint, no joint movements could be observed during the experiment, resulting in minimal, if any, changes in muscle length.

Dynamic Conditions (Cycling): Monopolar HD-sEMG signals were recorded from the Vastus Lateralis muscle of a
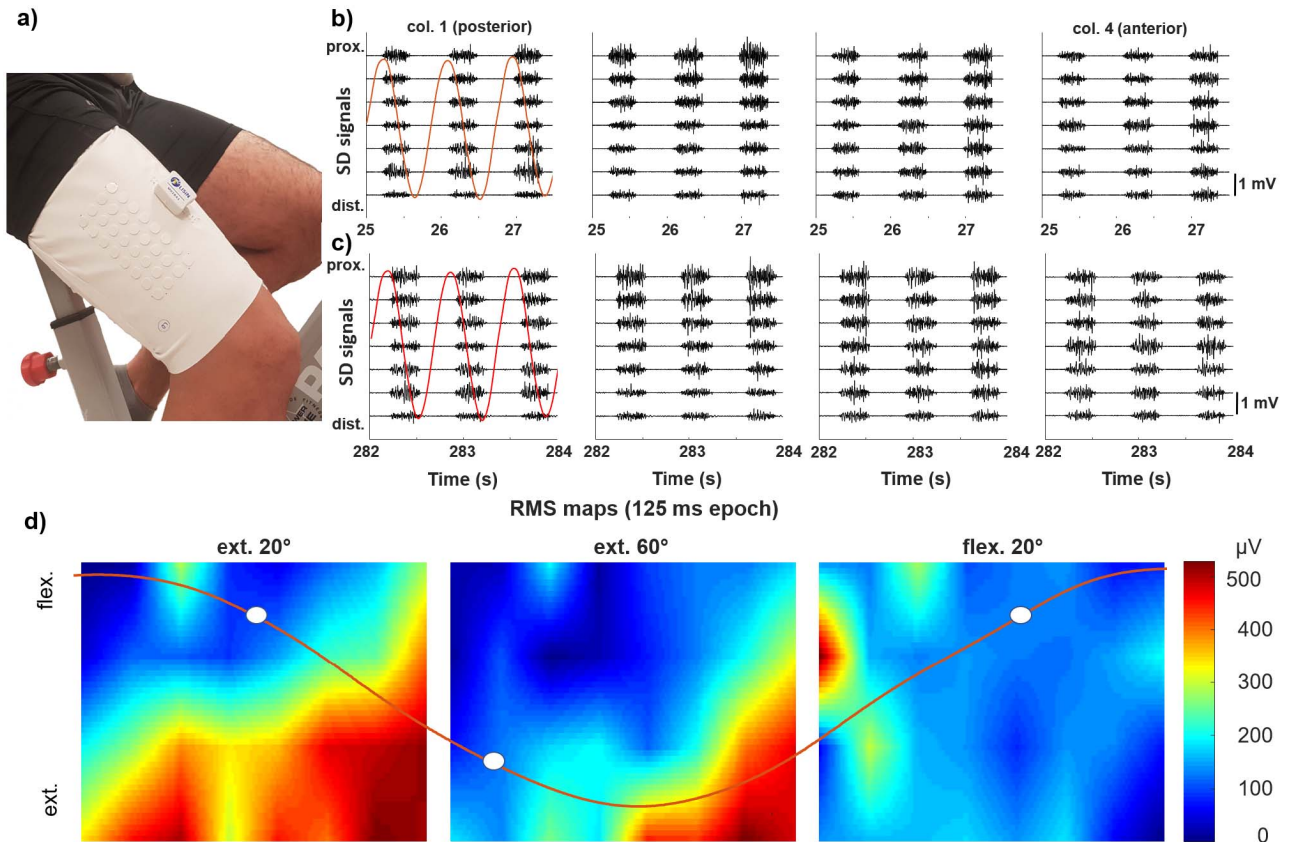
Fig. 7. Example of signals acquired during a cycling task. The subject was asked to cycle at 60 rpm for 10 min. Monopolar EMG signals were recorded from the Vastus Lateralis muscle a). Examples of single-differential signals are shown, created from monopolar signals collected during three cycles at the beginning b) and at the middle c) of the task. The quality of the signals is stable all along the contraction and no movement artefacts or interferences can be observed. The RMS maps calculated for the collected monopolar signals over three 125 ms long epochs, corresponding to different phases of cycling, are shown in d).

healthy subject (Male, Age 27, BMI 21.4) during cycling at 60 rpm using the textile grid of electrodes (8 rows × 4 columns, 15 mm inter-electrode distance; Figure 7.a). Skin was gently scrubbed with a medical grade abrasive paste (Nuprep, Weaver and Company, Aurora, USA). The textile grid was positioned on the skin using an elastic band wrapped on the subject's thigh in a comfortable way. The cycling phases were identified based on the knee joint-angle detected by an electro-goniometer connected to a system for the acquisition of biomechanical signals (DueBio, OT Bioelettronica, Italy). EMGs and angle data were recorded synchronously with a maximum synchronization delay smaller than 0.5 ms.

III. RESULTS AND DISCUSSION

The manufacturing of the electrode grid is based on state-of-the-art techniques and procedures (e.g. lamination and 3D-printing). The conductive electrodes/tracks are applied to the textile substrate using standard lamination techniques. The interconnection between the conductive tracks and the amplifier is obtained throughout a standard flexible PCB. A manual step is required for the connection of the flexible PCB to the conductive pads on the textile substrate but this could be automatized in a small production scenario.

A. Electrical, In-System, Characterization

Table I shows the mean and standard deviation of the components constituting the lumped parameters model described

TABLE I
VALUES OF THE LUMPED PARAMETERS MODEL OF THE TEXTILE TRACES (N = 96)

R (Ω)	L (nH)	C (nF)	f_0 (MHz)
33.10 ± 0.06	0.41 ± 0.12	371.29 ± 15.20	12.97 ± 0.55

Mean and standard deviation of the lumped parameters characterizing 96 textile traces.

in the methods. These values were calculated without any mechanical stress applied on three textile grids and averaged over all the traces (32 traces × 3 grids = 96 measurements) of the tested prototypes.

Given the values of resistance, capacitance and natural frequency of the lumped parameter model, it is possible to conclude that traces (whose impedances are in series with the electrode-skin impedances) do not affect the quality of the detected signals because, in the sEMG frequency band (10Hz - 500 Hz), their resulting impedances are negligible with respect to the electrode-skin impedance (Section 3.2).

The same tests were repeated during progressive stretching of the grids as described in the methods. No brakes in traces (open circuit condition) were observed for elongations shorter than 21 %, for which the resistive component of the impedance of all the 96 tested traces was lower than 1 kΩ. Above this elongation threshold, a sudden increase of the traces resistance was observed, indicating an on/off contact behavior similar

Condition	$|Z_{5\,Hz}|$ (kΩ) (MEDIAN [IQR])	$|Z_{50\,Hz}|$ (kΩ) (MEDIAN [IQR])
30 mmHg Pressure, no skin treatment	*481 [174, 823]*	*185 [96, 822]*
El. Sport Sleeve no skin treatment	*1385 [1223, 1660]*	*405 [347, 1660]*
30 mmHg Pressure, Abrasive Paste skin treatment	*172 [67, 450]*	*98 [51, 243]*
El. Sport Sleeve, Abrasive Paste skin treatment	*365 [254, 430]*	*146 [115, 430]*

to that observed when the common copper, non-textile, wires break. Considering the traces length (about 10 cm for each channel), this elongation corresponds to about 1.9 cm per trace. The experimental tests performed do not suggest such a level of stress during the experimental conditions.

However, it is difficult to predict weather this maximal elongation is sufficient to ensure a good stability of the signal transmission along the traces in most of the experimental contexts (i.e. changes in muscle and grid shape), as this depends on the muscle volume, contraction type and level. It is however possible to indicate that a safety choice is to align the traces longitudinally to the muscle to limit their elongation (Figure 6.a).

B. Electrode-Skin System Characterization

Table II summarizes the results of the electrodes-skin impedance measurements on the Biceps Brachii of two subjects in the four experimental conditions considered. In the no-skin-treatment condition, results show that the order of magnitude of the electrode-skin impedance at 5 Hz and 50 Hz (hundreds of kilo Ohms) does not change when the textile grid is fixed with an elastic sport sleeve with respect to the application of a constant 30 mmHg pressure by means of a blood pressure cuff.

After treating the skin with abrasive gel, we observed an overall reduction of the measured impedances (see median values in Table II), but most importantly, it is worth noting a marked reduction of the absolute variability (as shown by IQR values in Table II). The impedance variability across the electrodes of the detection system is a relevant parameter because it provides an estimate of the expected electrode-skin impedance unbalance between two electrodes of the grid. The large variability of the electrode-skin impedances observed for the no skin treated condition, may result indeed in high levels of power line interference detected in differential recordings [41], [51], [57]. Considering a biopotential amplifier, floating with respect to ground (i.e. battery powered) having 50 Hz input impedance $|Z_{i50Hz}| = 100$ MΩ

and a realistic common mode voltage at its inputs equal to $V_c = 10$ mV$_{RMS}$ (50 Hz), the input referred power line interference due to the electrode-amplifier system with an impedance unbalance ($|\Delta Z_{e50Hz}|$) of 726 kΩ (IQR corresponding to the 30 mmHg condition without skin treatment) would be equal to:

$$V_{IRN50} = V_c \frac{|\Delta Z_{e50Hz}|}{|Z_{i50Hz}|} = 73 \mu V_{RMS} \qquad (4)$$

Without skin treatment, the estimated maximum amount of power line interface is comparable to the RMS amplitude of the sEMG signal. Scrubbing the skin with abrasive paste lowers the median and IQR of the 50 Hz electrode-skin impedance by approximately 75 % in both cases. It is important to observe that in this case, the 50 Hz impedance unbalance between two electrodes used to collect differential sEMG signals could be highly reduced, with a proportional reduction of the maximum amount of power line interference. Figure 5 shows the distribution of electrode-skin impedance magnitude at 5Hz and 50Hz in one subject. It is possible to observe that the electrodes of column 4 have a higher impedance with respect to those of other columns. This observation shows that particular care shall be taken placing the textile grid to ensure that also the edges of the grid have a good contact with the skin, regardless of the skin treatment or pressure conditions.

The electrode-skin noise level, measured on all 32 electrodes, was 3 μV$_{RMS}$ $\pm$ 1 μV$_{RMS}$ considering all the reported experimental conditions and it resulted comparable with that observed in [36] using standard, flexible PCB-based grids of silver electrodes.

These results suggest that the proposed textile grid could guarantee a good quality of the collected sEMG signals after skin treatment [58], [59]. In the following section, an experimental validation based on sEMG signals detected using the developed detection system is reported.

C. sEMG Detection

1) Counter Gravity Isometric Contraction: Figure 6.b shows the Single Differential (SD) signals computed via software from the detected monopolar signals. It is possible to observe action potentials belonging to different motor units in different columns of the grid. It should be noted that conventional grids generally comprise smaller electrode-skin contact areas and shorter IEDs when compared to our textile grid. It would therefore appear reasonable to expect greater spatial differences between columns of electrodes [31], [38]. The propagation of action potentials can be observed along proximal and distal semi-fibers (Figure 6.c). The conduction velocity estimated with a multichannel estimation algorithm [60] from proximal channels (Figure 6.c) using epochs of 1s was 5.03 m/s [4.25-5.5] (Median [IQR]) with a cross-correlation of 0.75 [0.74-0.77], comparable to what obtained with standard wet electrodes [61], [62]. The contamination of power line interference is negligible, confirming that the quality of the electrode-skin contact described in the Paragraph 3.1 is acceptable. Finally, no artifacts were appreciated in the whole, recorded data, possibly resulting from any unobservable movement of the elbow joint taking place during this experiment.

2) Dynamic Contractions (Cycling): An example of signals recorded during cycling at 60 rpm is reported in Figure 7. The intermittent, temporal profile of sEMG amplitude is in agreement with what was expected [63]. No artefacts or interferences were observed along the whole cycling exercise. The quality of the signals and the absence of movement artefacts allow the study of muscle activity distribution during different cycling phases, as shown by the RMS maps (Figure 7.d).

We did not assess the effect of perspiration because it would be hard to say whether it would improve or not the performances of the proposed detection system. The perspiration issue applies to detection systems in general. For the textile-based detection system presented here, excessive perspiration could result in short circuit between adjacent electrodes. For the conventional detection systems, whereby grids are secured to the skin with adhesive pads, excessive perspiration leads to losing contacts between the grid and the skin. Although we acknowledge the need for future studies on this matter, experimental results presented here support the practical validity of the textile grid in different circumstances, from laboratory-controlled conditions to dynamic tasks.

IV. Conclusion

The aim of this work was to design, characterize, and test a wearable, HD-sEMG detection system based on a grid of 32 textile dry electrodes with 15 mm inter-electrode distance. The detection system was designed to meet the need for ease of wearing and use and manufacturability for small scale production.

The detection system was characterized in terms of electrical properties of the conductive traces and electrode-skin interface. The characterization of the conductive traces (96 traces tested) with a longitudinal stress applied showed no brakes in traces for elongations shorter than 21%. Our in-vivo tests suggested this figure is adequate to guarantee the integrity of the conductive traces. Further studies are required to test the usability of our detection system for contraction implying a high degree of stretching stresses on the detection system.

The electrode-skin impedance was investigated with and without scrubbing the skin with abrasive paste, while the skin treatment effect was investigated applying a 30 mmHg pressure to guarantee stable and repeatable conditions. The results of the electrode-skin impedance characterization suggested scrubbing the skin before applying the electrodes to reduce power line interference.

HD-sEMG signals were successfully collected during static and dynamic contractions. Recorded signals showed good quality and the possibility to estimate muscle fiber conduction velocity in a physiological range [49], [60], [61], [65]. During cyclic dynamic contractions lasting 10 min, HD-sEMG signals were stable during the whole task without movement artefacts.

In this work we focused the characterization of the proposed system on the aspects more strictly related with the signal detection (electrode-skin interface, conductive traces model, motion artefacts). Comfort-related aspects (e.g. breathability of the detection system) and issues of concern for the long-term monitoring of EMGs have not been approached and will be considered in future studies.

The developed detection system constitutes an advancement of the state-of-the-art technology for HD-sEMG acquisition systems and could be used as an enabling technology for the development of new applications requiring short-time preparation of the experimental setup, ease of use and high-quality sEMG signals.

References

[1] V. Agostini, M. Ghislieri, S. Rosati, G. Balestra, and M. Knaflitz, "Surface electromyography applied to gait analysis: How to improve its impact in clinics?" *Frontiers Neurol.*, vol. 11, p. 994, Sep. 2020.

[2] C. Castellini and P. van der Smagt, "Surface EMG in advanced hand prosthetics," *Biol. Cybern.*, vol. 100, no. 1, pp. 35–47, Jan. 2009.

[3] Y. Fu, J. Zhao, Y. Dong, and X. Wang, "Dry electrodes for human bioelectrical signal monitoring," *Sensors*, vol. 20, no. 13, p. 3651, Jun. 2020.

[4] Y. M. Chi, T.-P. Jung, and G. Cauwenberghs, "Dry-contact and noncontact biopotential electrodes: Methodological review," *IEEE Rev. Biomed. Eng.*, vol. 3, no. 1, pp. 106–119, 2010.

[5] L. Ren, B. Liu, W. Zhou, and L. Jiang, "A mini review of microneedle array electrode for bio-signal recording: A review," *IEEE Sensors J.*, vol. 20, no. 2, pp. 577–590, Jan. 2020.

[6] Y. Sun and X. B. Yu, "Capacitive biopotential measurement for electrophysiological signal acquisition: A review," *IEEE Sensors J.*, vol. 16, no. 9, pp. 2832–2853, May 2016.

[7] L. Tian *et al.*, "Large-area MRI-compatible epidermal electronic interfaces for prosthetic control and cognitive monitoring," *Nature Biomed. Eng.*, vol. 3, no. 3, pp. 194–205, Mar. 2019.

[8] L. M. Ferrari *et al.*, "Ultraconformable temporary tattoo electrodes for electrophysiology," *Adv. Sci.*, vol. 5, no. 3, 2018, Art. no. 1700771.

[9] Y. Wang *et al.*, "Electrically compensated, tattoo-like electrodes for epidermal electrophysiology at scale," *Sci. Adv.*, vol. 6, no. 43, Oct. 2020, Art. no. eabd0996.

[10] L. Guo, L. Sandsjö, M. Ortiz-Catalan, and M. Skrifvars, "Systematic review of textile-based electrodes for long-term and continuous surface electromyography recording," *Textile Res. J.*, vol. 90, no. 2, pp. 227–244, Jan. 2020.

[11] D. Pani, A. Achilli, and A. Bonfiglio, "Survey on textile electrode technologies for electrocardiographic (ECG) monitoring, from metal wires to polymers," *Adv. Mater. Technol.*, vol. 3, no. 10, Oct. 2018, Art. no. 1800008.

[12] R. Merletti and G. L. Cerone, "Tutorial. Surface EMG detection, conditioning and pre-processing: Best practices," *J. Electromyogr. Kinesiol.*, vol. 54, Oct. 2020, Art. no. 102440.

[13] G. Acar, O. Ozturk, A. J. Golparvar, T. A. Elboshra, K. Böhringer, and M. K. Yapici, "Wearable and flexible textile electrodes for biopotential signal monitoring: A review," *Electronics*, vol. 8, no. 5, p. 479, Apr. 2019.

[14] S. Yao, J. Yang, F. R. Poblete, X. Hu, and Y. Zhu, "Multifunctional electronic textiles using silver nanowire composites," *ACS Appl. Mater. Interfaces*, vol. 11, no. 34, pp. 31028–31037, Aug. 2019.

[15] D. Pani, A. Achilli, A. Spanu, A. Bonfiglio, M. Gazzoni, and A. Botter, "Validation of polymer-based screen-printed textile electrodes for surface EMG detection," *IEEE Trans. Neural Syst. Rehabil. Eng.*, vol. 27, no. 7, pp. 1370–1377, Jul. 2019.

[16] J. S. Michelsen, M. C. Lund, T. Alkjær, T. Finni, J. B. Nielsen, and J. Lorentzen, "Wearable electromyography recordings during daily life activities in children with cerebral palsy," *Develop. Med. Child Neurol.*, vol. 62, no. 6, pp. 714–722, Jun. 2020.

[17] A. Paiva, A. Catarino, H. Carvalho, O. Postolache, G. Postolache, and F. Ferreira, "Design of a long sleeve t-shirt with ECG and EMG for athletes and rehabilitation patients," in *Innovation, Engineering and Entrepreneurship* (Lecture Notes in Electrical Engineering). Cham, Switzerland: Springer, 2019.

[18] T. Finni, M. Hu, P. Kettunen, T. Vilavuo, and S. Cheng, "Measurement of EMG activity with textile electrodes embedded into clothing," *Physiolog. Meas.*, vol. 28, no. 11, pp. 1405–1419, Nov. 2007.

[19] T. Finni, M. Hu, P. Kettunen, T. Vilavuo, and S. Cheng, "Validity, reliability and feasibility of measuring muscle activity with textile electrodes embedded into clothing," *J. Biomech.*, vol. 40, p. S217, Jan. 2007.

[20] S. L. Colyer and P. M. McGuigan, "Textile electrodes embedded in clothing: A practical alternative to traditional surface electromyography when assessing muscle excitation during functional movements," *J. Sports Sci. Med.*, vol. 17, no. 1, p. 101, 2018.

[21] R. Di Giminiani, M. Cardinale, M. Ferrari, and V. Quaresima, "Validation of fabric-based thigh-wearable EMG sensors and oximetry for monitoring quadriceps activity during strength and endurance exercises," *Sensors*, vol. 20, no. 17, p. 4664, Aug. 2020.

[22] S. K. Lynn, C. M. Watkins, M. A. Wong, K. Balfany, and D. F. Feeney, "Validity and reliability of surface electromyography measurements from a wearable athlete performance system," *J. Sports Sci. Med.*, vol. 17, vol. 2, p. 205, 2018.

[23] F. Lorussi, N. Carbonaro, D. De Rossi, R. Paradiso, P. Veltink, and A. Tognetti, "Wearable textile platform for assessing stroke patient treatment in daily life conditions," *Frontiers Bioeng. Biotechnol.*, vol. 4, p. 28, Mar. 2016.

[24] B. Sumner, C. Mancuso, and R. Paradiso, "Performances evaluation of textile electrodes for EMG remote measurements," in *Proc. 35th Annu. Int. Conf. IEEE Eng. Med. Biol. Soc. (EMBC)*, Jul. 2013, pp. 6510–6513.

[25] D. Farina, T. Lorrain, F. Negro, and N. Jiang, "High-density EMG E-textile systems for the control of active prostheses," in *Proc. Annu. Int. Conf. IEEE Eng. Med. Biol. EMBC*, Aug. 2010, pp. 1–3.

[26] Z. Zhang, S. Liu, and G. Li, "Usability analysis of textile sensors in control of multifunction myoelectric prostheses," in *Proc. 4th Int. Conv. Rehabil. Eng. Assistive Technol. (i-CREATe)*, 2010, pp. 1–4.

[27] L. M. Arruda *et al.*, "Design and testing of a textile EMG sensor for prosthetic control," in *IoT Technologies for HealthCare* (Lecture Notes of the Institute for Computer Sciences, Social-Informatics and Telecommunications Engineering). Cham, Switzerland: Springer, 2020.

[28] S. Lee, M.-O. Kim, T. Kang, J. Park, and Y. Choi, "Knit band sensor for myoelectric control of surface EMG-based prosthetic hand," *IEEE Sensors J.*, vol. 18, no. 20, pp. 8578–8586, Oct. 2018.

[29] R. Di Giminiani *et al.*, "A wearable integrated textile EMG and muscle oximetry system for monitoring exercise-induced effects: A feasibility study," in *Proc. IEEE Int. Symp. Med. Meas. Appl. (MeMeA)*, Jun. 2018, pp. 1–5.

[30] G. Marco, B. Alberto, and V. Taian, "Surface EMG and muscle fatigue: Multi-channel approaches to the study of myoelectric manifestations of muscle fatigue," *Physiolog. Meas.*, vol. 38, no. 5, pp. R27–R60, May 2017.

[31] T. M. Vieira and A. Botter, "The accurate assessment of muscle excitation requires the detection of multiple surface electromyograms," *Exerc. Sport Sci. Rev.*, vol. 49, no. 1, pp. 23–34, Jan. 2021.

[32] S. F. Dick, K. U. Bert, L. G. Bernd, and V. D. P. Johannes, "High-density surface EMG: Techniques and applications at a motor unit level," *Biocybern. Biomed. Eng.*, vol. 32, no. 3, pp. 3–27, Jan. 2012.

[33] D. Farina, F. Negro, S. Muceli, and R. M. Enoka, "Principles of motor unit physiology evolve with advances in technology," *Physiology*, vol. 31, no. 2, pp. 83–94, Mar. 2016.

[34] R. Merletti and D. Farina, *Surface Electromyography: Physiology, Engineering and Applications*. Hoboken, NJ, USA: Wiley, 2016.

[35] I. Campanini, C. Disselhorst-Klug, W. Z. Rymer, and R. Merletti, "Surface EMG in clinical assessment and neurorehabilitation: Barriers limiting its use," *Frontiers Neurol.*, vol. 11, pp. 1–22, Sep. 2020.

[36] G. L. Cerone, A. Botter, and M. Gazzoni, "A modular, smart, and wearable system for high density sEMG detection," *IEEE Trans. Biomed. Eng.*, vol. 66, no. 12, pp. 3371–3380, Dec. 2019.

[37] M. Gazzoni, N. Celadon, D. Mastrapasqua, M. Paleari, V. Margaria, and P. Ariano, "Quantifying forearm muscle activity during wrist and finger movements by means of multi-channel electromyography," *PLoS One*, vol. 9, no. 10, pp. 1–11, 2014.

[38] R. Merletti and S. Muceli, "Tutorial. Surface EMG detection in space and time: Best practices," *J. Electromyography Kinesiol.*, vol. 49, Dec. 2019, Art. no. 102363.

[39] R. Merletti, A. Botter, A. Troiano, E. Merlo, and M. A. Minetto, "Technology and instrumentation for detection and conditioning of the surface electromyographic signal: State of the art," *Clin. Biomech.*, vol. 24, no. 2, pp. 122–134, Feb. 2009.

[40] J. G. Webster, *Medical Instrumentation-Application and Design*. Hoboken, NJ, USA: Wiley, 2013.

[41] A. C. M. van Rijn, A. Peper, and C. A. Grimbergen, "High-quality recording of bioelectric events: Part 1 interference reduction, theory and practice," *Med. Biol. Eng. Comput.*, vol. 28, no. 5, pp. 389–397, Sep. 1990.

[42] R. Merletti, "The electrode–skin interface and optimal detection of bioelectric signals," *Physiolog. Meas.*, vol. 31, no. 10, pp. 1–4, Oct. 2010.

[43] G. L. Cerone and M. Gazzoni, "A wireless, minaturized multi-channel sEMG acquisition system for use in dynamic tasks," in *Proc. IEEE Biomed. Circuits Syst. Conf. (BioCAS)*, Oct. 2017, pp. 1–4.

[44] A. Cömert, M. Honkala, and J. Hyttinen, "Effect of pressure and padding on motion artifact of textile electrodes," *Biomed. Eng. OnLine*, vol. 12, no. 1, p. 26, 2013.

[45] A. Cömert and J. Hyttinen, "Investigating the possible effect of electrode support structure on motion artifact in wearable bioelectric signal monitoring," *Biomed. Eng. OnLine*, vol. 14, no. 1, p. 44, May 2015.

[46] S. Majumder, T. Mondal, and M. J. Deen, "Wearable sensors for remote health monitoring," *Sensors*, vol. 17, no. 1, pp. 1–45, 2017.

[47] M. Stoppa and A. Chiolerio, "Wearable electronics and smart textiles: A critical review," *Sensors*, vol. 14, no. 7, pp. 11957–11992, Jul. 2014.

[48] J. G. Webster, "Reducing motion artifacts and interference in biopotential recording," *IEEE Trans. Biomed. Eng.*, vol. BME-31, no. 12, pp. 823–826, Dec. 1984.

[49] R. Merletti, A. Botter, C. Cescon, M. A. Minetto, and T. M. M. Vieira, "Advances in surface EMG: Recent progress in clinical research applications," *Crit. Rev. Biomed. Eng.*, vol. 38, no. 4, pp. 347–379, 2010.

[50] R. Gatzke, "The electrode: A measurement systems viewpoint," in *Biomedical Electrode Technology Theory and Practice*. New York, NY, USA: Academic, 1974, p. 447.

[51] J. C. Huhta and J. G. Webster, "60-Hz interference in electrocardiography," *IEEE Trans. Biomed. Eng.*, vol. BME-20, no. 2, pp. 91–101, Mar. 1973.

[52] G. Piervirgili, F. Petracca, and R. Merletti, "A new method to assess skin treatments for lowering the impedance and noise of individual gelled Ag–AgCl electrodes," *Physiolog. Meas.*, vol. 35, no. 10, pp. 2101–2118, Oct. 2014.

[53] R. Merletti and P. Parker, *Electromyography: Physiology, Engineering, and Noninvasive Applications*. Hoboken, NJ, USA: Wiley, 2004.

[54] T. Yamamoto and Y. Yamamoto, "Non-linear electrical properties of skin in the low frequency range," *Med. Biol. Eng. Comput.*, vol. 19, no. 3, pp. 302–310, May 1981.

[55] P. Cattarello and R. Merletti, "Characterization of dry and wet electrode-skin interfaces on different skin treatments for HDsEMG," in *Proc. IEEE Int. Symp. Med. Meas. Appl. (MeMeA)*, May 2016, pp. 1–6.

[56] A. Botter, T. M. M. Vieira, I. D. Loram, R. Merletti, and E. F. Hodson-Tole, "A novel system of electrodes transparent to ultrasound for simultaneous detection of myoelectric activity and B-mode ultrasound images of skeletal muscles," *J. Appl. Physiol.*, vol. 115, no. 8, pp. 1203–1214, Oct. 2013.

[57] B. B. Winter and J. G. Webster, "Reduction of interference due to common mode voltage in biopotential amplifiers," *IEEE Trans. Biomed. Eng.*, vol. BME-30, no. 1, pp. 58–62, Jan. 1983.

[58] R. Merletti, B. Afsharipour, and G. Piervirgili, "High density surface EMG technology," in *Converging Clinical and Engineering Research on Neurorehabilitation*. Berlin, Germany: Springer, 2013, pp. 1205–1209.

[59] P. Cattarello, S. D. H. Soedirdjo, B. Afsharipour, and R. Merletti, "Effect of electrode size on amplitude estimation of HDsEMG maps," in *Converging Clinical and Engineering Research on Neurorehabilitation II*. Cham, Switzerland: Springer, 2017, pp. 1013–1017.

[60] D. Farina, E. Fortunato, and R. Merletti, "Noninvasive estimation of motor unit conduction velocity distribution using linear electrode arrays," *IEEE Trans. Biomed. Eng.*, vol. 47, no. 3, pp. 380–388, Mar. 2000.

[61] W. Li and K. Sakamoto, "Distribution of muscle fiber conduction velocity of M. Biceps Brachii during voluntary isometric contraction with use of surface array electrodes," *Appl. Hum. Sci. J. Physiolog. Anthropol.*, vol. 15, no. 1, pp. 41–53, 1996.

[62] D. Farina, D. Zagari, M. Gazzoni, and R. Merletti, "Reproducibility of muscle-fiber conduction velocity estimates using multichannel surface EMG techniques," *Muscle Nerve*, vol. 29, no. 2, pp. 282–291, 2004.

[63] M. Jorge and M. L. Hull, "Analysis of EMG measurements during bicycle pedalling," *J. Biomech.*, vol. 19, no. 9, pp. 683–694, 1986.

[64] A. Botter, F. Lanfranco, R. Merletti, and M. Minetto, "Myoelectric fatigue profiles of three knee extensor muscles," *Int. J. Sports Med.*, vol. 30, no. 6, pp. 408–417, Jun. 2009.